Supplementary Information

Optoelectronic Synapses Based on Hot-Electron-Induced Chemical Processes

Pan Wang, Mazhar E. Nasir, Alexey V. Krasavin, Wayne Dickson and Anatoly V. Zayats**

Department of Physics and London Centre for Nanotechnology, King's College London, Strand, London WC2R 2LS, UK

Correspondence to: pan.wang@kcl.ac.uk, a.zayats@kcl.ac.uk

S1. Fabrication of plasmonic nanorod metamaterials

The plasmonic nanorod metamaterials were fabricated by electrodeposition of Au into substrate-supported porous alumina templates. The substrate is a multilayered structure comprised of a glass slide (0.7 mm in thickness), a tantalum oxide adhesive layer (10 nm in thickness), and an Au film (7 nm in thickness) acting as a working electrode for the electrochemical reaction. An aluminum film (~500 nm in thickness) is deposited onto the substrate by planar magnetron sputtering and is subsequently anodized in oxalic acid (0.3 M) at 40 V to produce the porous alumina template by two-step anodization. The diameter, separation and ordering of the Au nanorods in the assembly are controlled by the conditions of the anodization. The electrodeposition of Au is performed with a three-electrode system using a non-cyanide solution. The length of the Au nanorods is controlled by the electrodeposition time. In this work, the length of the Au nanorods is slightly shorter than the height of the alumina template. The metamaterials were then washed several times in deionized water (DI water) and stored in 200 proof ethanol for future use. Figure S1 shows a typical SEM image of a Au nanorod metamaterial, the white dots correspond to the tips of the Au nanorods.

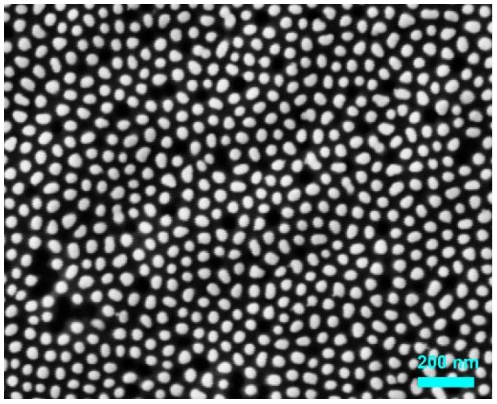

Figure S1. SEM image of the Au nanorod metamaterial.

S2. Fabrication of metal-polymer-metal tunnel junctions

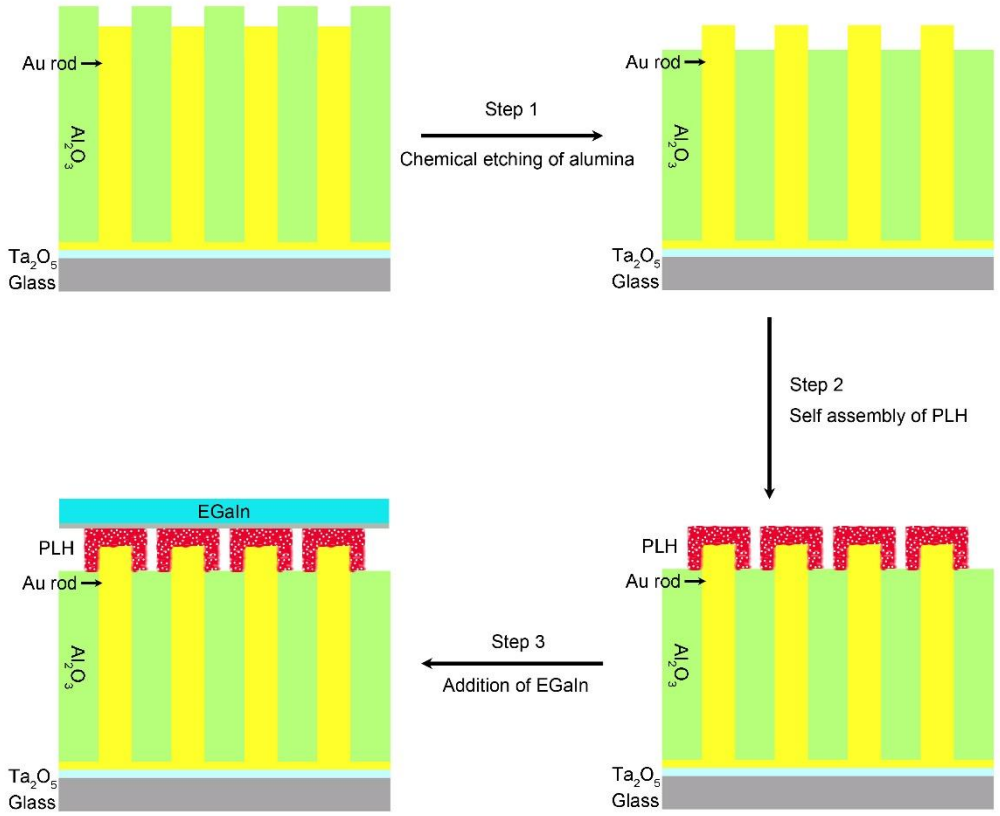

Figure S2. Schematic diagram showing the steps for the fabrication of metal-polymer-metal tunnel junctions.

Figure S2 shows the schematic diagram of the fabrication of metal-polymer-metal tunnel junctions based on a plasmonic nanorod metamaterial. In the first step, a wet chemical etching method was used to remove some of the alumina matrix to make the tips of the Au nanorods slightly higher than the surrounding alumina. The nanorod metamaterial stored in ethanol was first dried under N_2 and then put into an aqueous solution of H_3PO_4 (3.5 %) at 35 °C to start the etching. The etching depth can be precisely controlled by the etching time. After the chemical etching, the metamaterial was washed several times in DI water.

In the second step, the exposed Au nanorod tips were functionalized with a monolayer of poly-L-histidine (PLH, Mw 5,000-25,000, Sigma-Aldrich). The etched nanorod metamaterial was

submerged into a PLH solution (1 mg/mL, pH ~5–6) and incubated for 0.5 h. Due to the high affinity of PLH to the Au surface and the positive charging of protonated PLH in the solution, a monolayer of PLH self-assembled onto the exposed Au nanorod tips. The metamaterial was then washed several times in DI water to remove weakly bound PLH and dried under N_2.

Finally, a droplet of EGaIn was added onto the surface of the nanorod metamaterial to form an array of metal-PLH-metal tunnel junctions. Two Au wires were connected to the bottom Au film and the EGaIn droplet for the application of a bias across the tunnel junctions (Figure S3).

S3. Nanorod-metamaterial-based tunnelling device

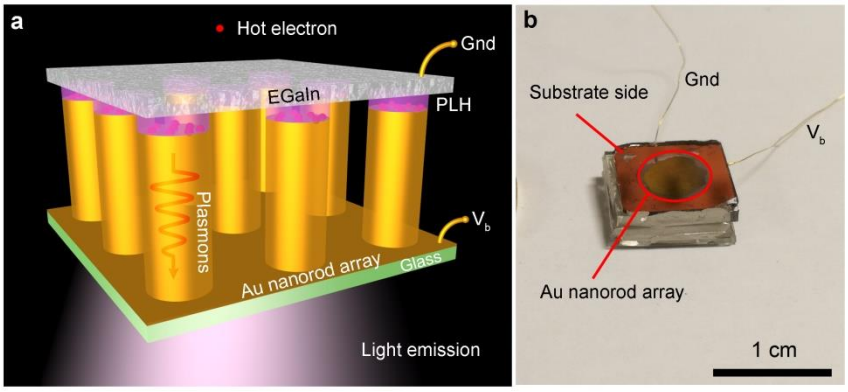

Figure S3. **a**, Schematic diagram of the tunneling junction array constructed on a Au nanorod metamaterial. **b**, Photograph of a nanorod-metamaterial-based tunnel device.

S4. Estimation of operation power for single tunnel junctions

Under a forward bias of 2.5 V, the total tunnelling current through the device is around 0.09 A. Considering a tunnel junction area of ~4 mm^2 and a nanorod density of ~10^{10} cm^{-2}, the tunnelling current through a single nanorod is ~225 pA. In this case, the operation power for a single memristive plasmonic tunnel junction is ~600 pW.

S5. Estimation of inelastic tunnelling efficiency

In the nanorod-metamaterial-based tunnel junctions, the light emission is due to the radiative decay of plasmonic modes excited by the inelastic tunnelling electrons. In this case, the relation between inelastic tunnelling efficiency ($\eta_{inel} = \Gamma_{inel}/\Gamma_{tot}$, where Γ_{inel} and Γ_{tot} are the inelastic and total tunnelling rates, respectively) and electron-to-photon conversion efficiency ($\eta_{el-phot}$) can be written as: $\eta_{el-phot} = \eta_{inel} \cdot \eta_{ant}$, where η_{ant} is the antenna radiation efficiency ($\eta_{ant} = P_{rad}/P_{tot}$, defining how much power from the excited plasmonic modes is radiated in light, where P_{tot} is the total power flow emitted by a dipole representing the tunneling current source[1,2], and P_{rad} is the power low fraction carried away by photons, integrated in the substrate, both determined in a purpose-built numerical simulation). The electron-to-photon conversion efficiency can be estimated from the ratio of emitted photons (evaluated from the measured emission power, assuming that all the emitted photons have the same wavelength of 850 nm) to injected electrons (evaluated from the measured tunnelling current under a 2.5 V forward bias) during each period of measurement. The antenna radiation efficiency η_{ant} can be evaluated from the numerical simulations to be ~3.5×10^{-4} at 850 nm. One can plot the evolution of the inelastic tunnelling efficiency during the memristor programming process using the formula: $\eta_{inel} = \eta_{el-phot}/\eta_{ant}$ (Figure 2c,f).

S6. Non-volatility of the device

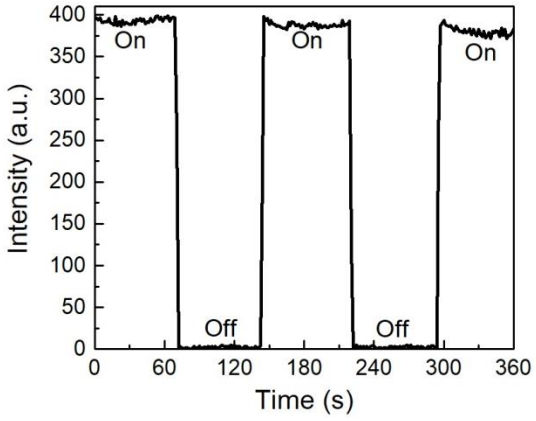

Figure S4. Emission intensity of the device (at Level H) monitored at 850-nm wavelength when the bias is switched on (2.5 V) and off (0 V).

S7. Numerical simulations

Numerical simulations of the near-field distributions of the electric field inside the nanorod metamaterial and the associated electric current in the nanorods were performed using a finite element method (Comsol Multiphysics software). The metamaterial was illuminated from the substrate side by a plane wave at an angle of incidence of 45º. The distribution of the nanorods in the metamaterial was approximated with a square array, which allowed to simulate the entire system modeling a unite cell with properly defined Floquet boundary conditions on the unit cell sides, determined by a phase delay acquired by the incident plane wave while travelling between the corresponding faces. To ensure the absence of back-reflection, a perfectly matched layer was implemented on the illumination side. At the opposite (EGaIn) side, this was not needed due to metallic nature of the latter. Experimentally measured data with a mean free path correction of 3 nm, related to the properties of electrochemical deposition, were used for gold[3], experimental tabulated data was also used for the Al_2O_3 matrix[4], SiO_2 substrate[5] and Ta_2O_5 adhesion layer[6]. Optical properties of EGaIn were approximated by the Drude model

($\varepsilon_{EGaIn} = \varepsilon_\infty - \omega_p^2/(\omega^2 + i\gamma\omega)$, with high-frequency optical constant $\varepsilon_\infty = 1.08$, plasma frequency $\omega_p = 13.5$ eV and scattering rate $\gamma = 1.05$ eV)[7], while refractive indices of gallium oxide, naturally appearing on the EGaIn surface, and PLH polymer were taken as non-dispersive in the studied wavelength range and equal to 1.89 and 1.565, respectively.

References

1. Johansson, P. Light emission from a scanning tunneling microscope: Fully retarded calculation. Phys. Rev. B **58,** 10823–10834 (1998).
2. Rendell, R. W. & Scalapino, D. J. Surface plasmons confined by microstructures on tunnel junctions. Phys. Rev. B **24,** 3276–3294 (1981).
3. Johnson, P. B. & Christy, R. W. Optical constants of the noble metals. *Phys. Rev. B* **6,** 4370–4379 (1972).
4. Malitson, I. H. & Dodge, M. J. Refractive index and birefringence of synthetic sapphire. *J. Opt. Soc. Am.* **62,** 1405 (1972).
5. Malitson, I. H. Interspecimen comparison of the refractive index of fused silica. *J. Opt. Soc. Am.* **55,** 1205-1209 (1965).
6. Bright, T. J., Watjen, J. I., Zhang, Z. M., Muratore, C., Voevodin, A. A., Koukis, D. I., Tanner, D. B. & Arenas, D. J. Infrared optical properties of amorphous and nanocrystalline Ta_2O_5 thin films. *J. Appl. Phys.* **114,** 083515 (2013).
7. Blaber, M. G., Engel, C. J., Vivekchand, S. R. C., Lubin, S. M., Odom, T. W. & Schatz, G. C. Eutectic liquid alloys for plasmonics: theory and experiment. *Nano Lett.* **12,** 5275–5280 (2012).